 doi:10.20944/preprints202011.0200.v1

Article

Neural modelling of APS thermal spray process parameters for optimising the hardness, porosity and cavitation erosion resistance of Al_2O_3 -13% TiO_2 coatings

Mirosław Szala [1,*], Leszek Łatka [2], Michał Awtoniuk [3,*], Marcin Winnicki [2] and Monika Michalak [2]

[1] Department of Materials Engineering, Faculty of Mechanical Engineering, Lublin University of Technology, Nadbystrzycka 36D, Lublin 20-618, Poland; m.szala@pollub.pl
[2] Faculty of Mechanical Engineering, Wrocław University of Science and Technology, 5 Łukasiewicza Street, Wrocław 50-371, Poland; leszek.latka@pwr.edu.pl, marcin.winnicki@pwr.edu.pl, monika.michalak@pwr.edu.pl
[3] Warsaw University of Life Sciences, Institute of Mechanical Engineering, Nowoursynowska 164, 02-787 Warsaw, Poland; michal_awtoniuk@sggw.edu.pl
* Correspondence: m.szala@pollub.pl (M.S.); michal_awtoniuk@sggw.edu.pl (M.A.);

Abstract: The study aims to elaborate a neural model and algorithm for optimising hardness and porosity of coatings and thus ensure that they have superior cavitation erosion resistance. Al_2O_3-13wt.%TiO_2 ceramic coatings were deposited onto 316L stainless steel by atmospheric plasma spray (ASP). The coatings were prepared with different values of two spray process parameters: the stand-off distance and torch velocity. Microstructure, porosity and microhardness of the coatings were examined. Cavitation erosion tests were conducted in compliance with the ASTM G32 standard. Artificial neural networks (ANN) were employed to elaborate the model, and the multi-objectives genetic algorithm (MOGA) was used to optimise both properties and cavitation erosion resistance of the coatings. Results were analysed with Matlab software by Neural Network Toolbox and Global Optimization Toolbox. The fusion of artificial intelligence methods (ANN+MOGA) is essential for future selection of thermal spray process parameters, especially for the design of ceramic coatings with specified functional properties. Selection of these parameters is a multicriteria decision problem. The proposed method made it possible to find a Pareto front, i.e. trade-offs between several conflicting objectives – maximising the hardness and cavitation erosion resistance of Al_2O_3-13%TiO_2 coatings and, at the same time, minimizing their porosity.

Keywords: artificial neural network; APS; cavitation erosion; ceramic coatings; multi-objectives optimization; wear; hardness; microstructure; alumina – titania; Al_2O_3-13%TiO_2.

1. Introduction

Thermal spraying (TS) is an important technology used in the field of surface engineering. It is used to apply coatings to different types of materials (metals, ceramics, cermet). New methods and materials have been studied, improved and developed for over a century [1–3]. Among other methods, plasma spraying, or more precisely – atmospheric plasma spraying (APS), is the most widely used TS technique owing to its numerous advantages such as good adhesion strength, high plasma jet temperature and relatively high deposition rate [1]. The quality and properties of coatings depend to different degrees upon APS process parameters. For a more effective development of coatings it is necessary to understand the underlying physical processes and correlations between process parameters and coating characteristics [4,5]. Among others, the most important parameters include electrical power, spray distance and torch velocity [6–8]. A detailed description of APS as well as additional information about this technique can be found e.g. in [9,10].

 doi:10.20944/preprints202011.0200.v1

Simulations are a popular method of in-depth analysis of engineering processes. However, to carry out a simulation, one needs a model of the analysed process. Two main groups of models can be distinguished in modelling: physical models and those based on parametric identification. Physical models, so-called white box models, use the laws of physics to describe particular phenomena. These models are also referred to as analogue models [11,12]. They consider the energy balance, flows of heat and mass transfer as well as mutual interactions among them. Such models require a large number of parameters to be considered. An example of using white box models in APS modelling is given in [4]. For a modelling approach it is, therefore, reasonable to reduce the number down to a few parameters. This condition is satisfied by parametric models, also known as black box models [13]. The most popular tool for black box modelling is artificial neural network (ANN). Such models describe the mathematical relationship between input and output signals. Unlike white box models, they are built on the basis of experimental data rather than the laws of physics. An extensive description of APS neural modelling is presented in [5].

There is a continual demand for optimisation of spray parameters to ensure the required functional properties of fabricated coatings, particularly their resistance to different deterioration processes such as abrasion, corrosion or erosion. Although there are many studies on wear processes occurring in APS coatings, the problem of cavitation erosion (CE) has not been exhaustively investigated. Few definitions of this phenomenon are available, under which CE is described as a process of material degradation due to harmful fluid action initiated by pressure fluctuations in the liquid. When the liquid pressure drops, the vapour can grow, and as the pressure increases, the vapour bubbles implode. The resulting emission of shock waves and liquid-jet cause degradation of a solid material. Although the deterioration of materials is primarily mechanical in nature, it can be substantially accelerated by the presence of corrosion [14,15], solid particles [16–18], or both [16,19,20]. Furthermore, there is a wide choice of cavitation erosion resistance (CER) evaluation methods available in the literature. They pertain to the use of either standard test rigs under ASTM G32 (vibratory apparatus) [21,22] and ASTM G134 (cavitating liquid jet) [23,24] or non-standard solutions such as rotation discs and cavitation tunnel rigs [25–27]. However, the determination of complete cavitation curves by laboratory testing is usually very time-consuming. Therefore, various attempts have been made to shorten the testing time or reduce the number of test samples. For example, the process of CER estimation can be simplified by limiting the analysis to the incubation stage of erosion [28–31]. Overall, there is a demand for corelating the mechanical and functional properties of engineering materials with their CER. Different methods are employed to this end, starting from simple comparative analyses [32–34] and regression methods [4,35,36] to artificial neural networks [37,38]. Although comparative analyses into the relationship between plasma spray parameters and CER are reported in the literature [39,40], to our knowledge, no study to date has utilized the ANN to predict the CER of APS thermally sprayed coatings. Therefore, not only does this study investigate the relationship between spray process parameters and coating material properties, but it also makes use of ANN to preliminarily optimise the APS process parameters in order to obtain superior CER of the deposited ceramic coatings. Moreover, few studies have undertaken modelling the CER of Al_2O_3-13%TiO_2 ceramic coatings.

This study is a novel attempt at optimising atmospheric plasma spray parameters for Al_2O_3-13%TiO_2 ceramic coatings to ensure that they have the required functional properties, namely – porosity and hardness. Particularly, in this study we propose a new model and optimisation procedure for spray parameters selection to obtain coatings with superior cavitation erosion resistance.

The relationship between technological parameters and properties and cavitation wear resistance of coatings is a complex problem, one that requires the use of non-linear models such as neural networks. The properties of thermally sprayed coatings are interdependent. Results of our previous studies, e.g. on Al_2O_3-13%TiO_2 ceramic coatings, show that while these coatings have low hardness, they also present high porosity and thus are more prone to cavitation damage. For this reason, when searching for optimal technological parameters to ensure required functional properties, a multi-criteria optimisation algorithm should be used.

 doi:10.20944/preprints202011.0200.v1

This work is a continuation of our previous studies on the optimisation of structural materials and ceramic coatings to obtain the required functional properties [38,40,41]. This study proposes a model and optimisation procedure for selecting spray parameters ensuring coatings with specified functional properties. Calculations made in this work use the results obtained in our previous study [40] on APS Al_2O_3-13%TiO_2 coatings.

The main goal of this study is to elaborate a neural model and algorithm for optimising the porosity and hardness of Al_2O_3-13%TiO_2 coatings, and thus ensure that they have superior cavitation erosion resistance. The original ANN procedure is essential for future selection of thermal spray process parameters, especially for the design of ceramic coatings with specified functional properties.

2. Materials and Methods

2.1. Atmospheric plasma spray process parameters

In this study Al_2O_3-13wt% TiO_2 ceramic coatings were deposited onto 316L stainless steel by atmospheric plasma spray. The coatings were fabricated using different values of selected APS process parameters, namely – the stand-off distance (h) and torch velocity (V), **Table 1**. As it was mentioned in the introduction, these are key parameters with respect to functional properties. To ensure reliable results, the plan of experiment was based on the 2^k+1 type design of experiment (DoE), according to [42]. The samples were 25 mm in diameter and 2 mm in thickness. The APS process was performed with the SG100 plasma torch (Praxair, IN, USA) that was mounted on a 6-axis industrial robot, Fanuc 2000 IA. Two gases were used in plasma spraying: argon (to ignite the arc) and hydrogen (to improve electrical power of the arc). The deposition process was robotized to control all essential parameters and to ensure repeatability.

Table 1. Sample codes and APS process variables.

Sample code	Stand-off distance, h (mm)	Torch velocity, V ($mm \cdot s^{-1}$)
AT13-1	80	300
AT13-2	80	500
AT13-3	90	400
AT13-4	100	300
AT13-5	100	500

2.1. Investigation into the functional properties of Al_2O_3-13%TiO_2 coatings

The hardness H (HV0.1) and porosity P (%) of the coatings were evaluated according to the procedures described in our previous papers [43–45] while obtained results were discussed in detail in [40]. Cavitation erosion resistance (CER) tests were conducted according to the ASTM G32 standard [46] using the vibratory test rig described in [32,40]. The CER tests were performed by the stationary specimen method, with the gap between the horn tip and specimen surface set equal to 1 mm. The tests were conducted on the as-sprayed surfaces of Al_2O_3-13%TiO_2 coatings. The coatings had a roughness of Sa=5.4-6.2 μm. The cavitation test was repeated three times for every coating deposited with the specified spray parameters, as given in **Table 1**. Although detailed CER results were reported in our previous study [40], this work presents original erosion rate vs time curves, and the mean depth of erosion (MDE) is utilized for ANN modelling. The cavitation-worn specimens were compared with the undamaged surfaces by scanning electron microscopy in SEM-BSD mode.

2.1. Modeling and optimisation procedures - artificial neural network (ANN) and multi-objectives genetic algorithm (MOGA)

The neural model was developed using the Neural Network Toolbox in the Matlab environment (2017a). A block diagram of the model is shown in Figure 1. In the model we considered 2 input

Preprints (www.preprints.org) | NOT PEER-REVIEWED | Posted: 4 November 2020 doi:10.20944/preprints202011.0200.v1

signals, i.e. the stand-off distance h [mm] and torch velocity V (mm·s^{-1}), and 3 output signals, i.e. the hardness H (HV0.1), porosity P (%) and mean depth of erosion MDE (μm).

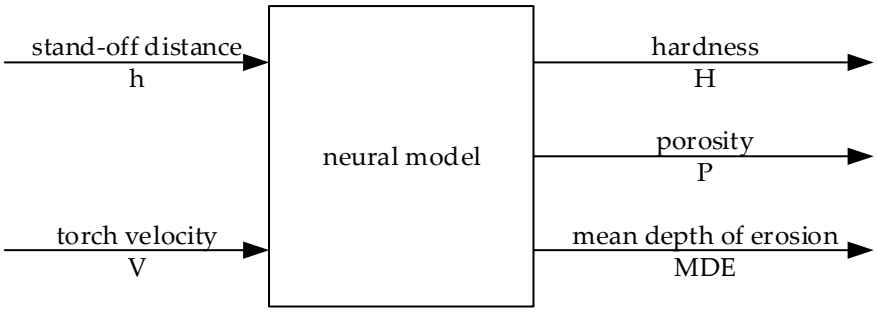

Figure 1. Block diagram of the analysed neural model.

The neural model has a layered structure and consists of an input layer, a hidden layer and an output layer. Each layer is assigned a specific number of neurons. For example, the model marked as 2-5-3 stands for a network with 2 input neurons, 5 hidden neurons and 3 output neurons. The number of signals used in modelling determines the number of input and output neurons. The selected number of hidden neurons is the decision-making parameter. In our study, we selected the number of hidden neurons in an experimental way by assessing the performance of networks with different structures. Details of this analysis are described in the Results and Discussion section. We have used the Levenberg-Marquardt backpropagation algorithm to train the network. The maximum number of epochs to train the network was set equal to 40. Since our dataset was limited to 5 samples only, we decided to perform k-fold cross validation. We assumed that $k = n$, so it is a type of the so-called leave-one-out cross validation [47].

We used root mean square error NRMSE (which is informally known as fit – and this name is used throughout the manuscript) as a model performance evaluation index. The model describes this phenomenon in a more detailed way if the fit value is higher. The fit index is calculated as follows:

$$fit = \left(1 - \frac{\|y - \hat{y}\|_2}{\|y - \bar{y}\|_2}\right) \cdot 100\% \quad (1)$$

where y is the output signal (measured), $\hat{y}$ is the predicted output signal, $\bar{y}$ is the mean output signal (measured).

Next, we used the neural model to find optimal APS thermal spray parameters. The process was optimised using a multi-objectives genetic algorithm implemented in the Global Optimisation Toolbox. The vector of decision variables x was

$$x = [h, V]^T \quad (2)$$

The selection of these parameters is a multicriteria decision problem. The proposed method made it possible to find a Pareto front, i.e. a trade-off between several conflicting objectives; in this particular case it was maximising the hardness and cavitation erosion resistance of analysed coatings and, at the same time, minimizing their porosity. Our goal was to find the vector x*

$$x^* = [h^*, V^*]^T, \quad (3)$$

which would satisfy the inequality constraints

$$\begin{aligned} 80 \le h \le 100, \\ 300 \le V \le 500, \end{aligned} \quad (4)$$

and would optimize the complex objective vector function J

$$J(x) = [\max H(x), \min P(x), \min MDE(x)]^T \quad (5)$$

The set of x* will form the Pareto front if there exists no vector x which satisfies the constraints (4) and at the same time optimizes each element of the objective vector function (5). The main MOGA

Preprints (www.preprints.org) | NOT PEER-REVIEWED | Posted: 4 November 2020 doi:10.20944/preprints202011.0200.v1

parameters were as follows: the number of generations – 200; population size – 50; selection type – tournament; crossover probability – 0.8.

3. Results and discussion

3.1. Properties and cavitaion erosion damage of the coatings

Surface morphology and cross-sectional microstructure of the Al_2O_3-13%TiO_2 ceramic coatings are shown in **Figure 2.** APS deposited Al_2O_3-13%TiO_2 coatings: surface morphology and cross section microstructure of AT13-2 (**a, b**) and AT13-5 (**c, d**), SEM-BSD., while their hardness and porosity results are given in **Table 2**. CER results of the specimens are summarised in **Figure 3**, while cavitation-damaged surfaces are shown in **Figure 4**. The microstructure and as-sprayed surface morphology of the fabricated APS coatings is typical of thermally sprayed coatings [48–50]. An analysis of the images in **Figures 2a, c** clearly shows the presence of lamellar splats, porosity, unmelted feedstock powder particles of a semi-spherical shape, and cracks in the ceramic lamellas. Every splat consists of columnar crystals, which is characteristic of APS deposited ceramics [40,51,52]. The coating adheres well to the substrate, and continuous bonding between the stainless substrate and ceramic coatings is visible. The results demonstrate that the coating porosity and hardness depend on the applied process parameters. According to our previous study [40], the decrease in hardness results from a less compact microstructure and lower degree of well molten particles. The hardness of the coatings is in range of 885-1235 HV0.1 (see **Table 2**) while their porosity ranges from 5.59 to 2.3 %. It can be concluded that the coatings are characterised by a relatively dense microstructure (see the cross sections in **Figure 2.** APS deposited Al_2O_3-13%TiO_2 coatings: surface morphology and cross section microstructure of AT13-2 (**a, b**) and AT13-5 (**c, d**), SEM-BSD.b and d), which proves that the spray process parameters were selected and set in a proper range.

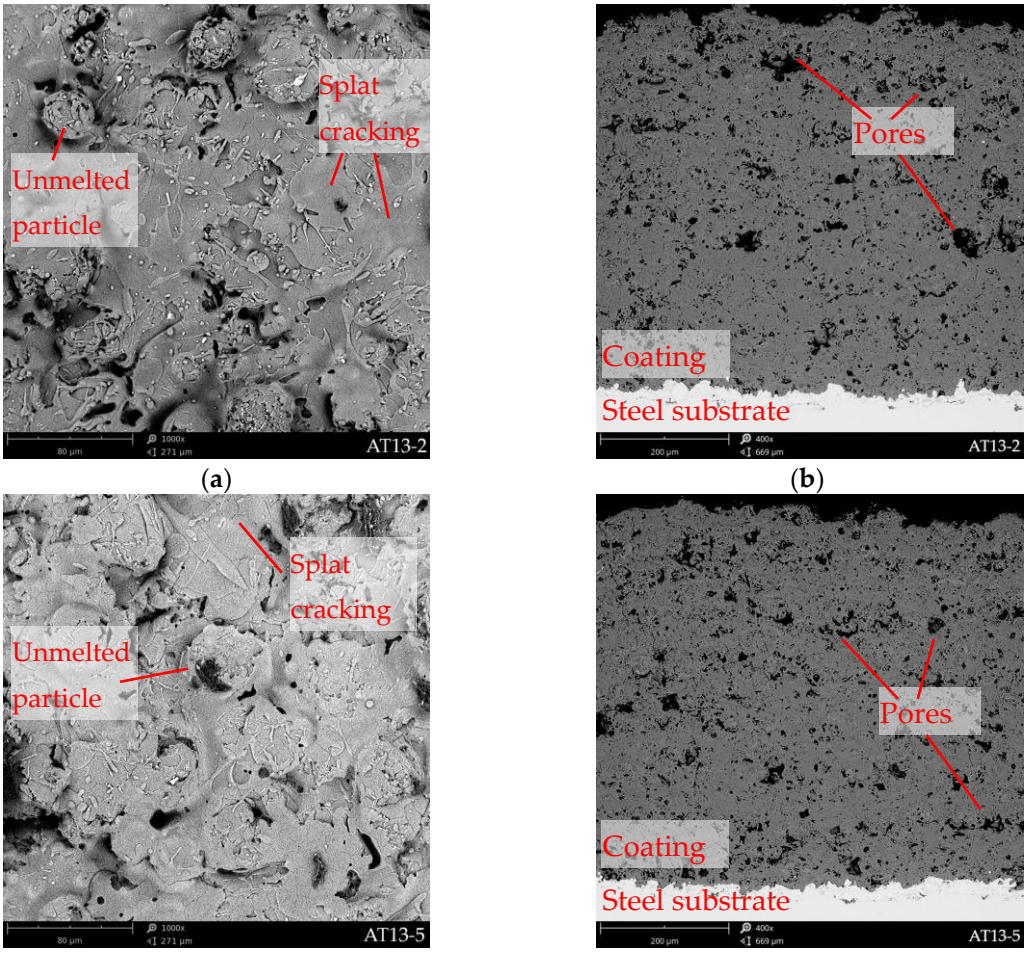

Preprints (www.preprints.org) | NOT PEER-REVIEWED | Posted: 4 November 2020 doi:10.20944/preprints202011.0200.v1

Figure 2. APS deposited Al_2O_3-13%TiO_2 coatings: surface morphology and cross section microstructure of AT13-2 (**a, b**) and AT13-5 (**c, d**), SEM-BSD.

Table 2. Properties of the Al_2O_3-13%TiO_2 coatings used in the ANN calculations, average ±SD.

Sample code	Hardness, H (HV0.1)	Porosity, P (%)
AT13-1	1237±105	2.30±0.37
AT13-2	885±108	5.59±0.63
AT13-3	1059±112	2.91±0.51
AT13-4	1028±118	4.28±0.60
AT13-5	984±108	4.16±0.57

The quantitative cavitation results demonstrate that the highest CER is shown by the AT13-3 specimens (see **Figure 3**) which obtained the lowest erosion rate and MDE. The damage process of all coatings is characterised by the maximal initial wear rate that decelerates after 10 minutes of testing. After approx. 2 h of testing, the wear rate decreases at a constant rate. The initial high wear rate of the coating material results from the "cleaning effect". It relies on the removal of loose material, surface non-uniformities, material discontinuities (e.g. partly melted particles) and the spallation of splat-edges. This effect can be observed not only for ceramic coatings but also for HVOF nickel- and cobalt-based coatings and cold-sprayed MMC [32,43]. The lowest erosion rate is observed for the AT13-3 coating (**Figure 3**a) and results from the low porosity of the coating and is a result of spraying parameters: h = 90 mm and V = 400 m/s, see **Table 2**. Material discontinuities such as pores act as the centres of material removal. The applied plasma spraying parameters do not affect the cavitation erosion mechanism. The erosion process is dominated by the removal of fragmented splats progressing into more deeply located lamellas and is accompanied by pit formation (**Figure 4**a and b). The presence of structural non-uniformities in the coatings accelerates the wear process and material removal, ending up with crater formation and exposition of the stainless steel substrate. The cavitation erosion behaviour of all deposited specimens relies on brittle fracture propagating through the columnar structure of the lamellas, see **Figure 4**c and d. Although in the previously mentioned work [40] the relationship between spray parameters and cavitation erosion indicators could not be calculated mathematically, this study uses the ANN to solve this problem.

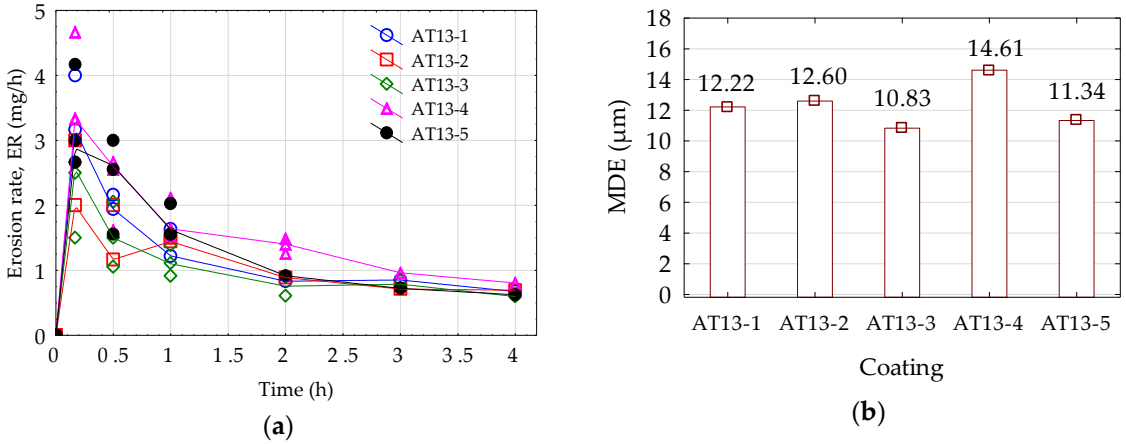

Figure 3. Cavitation erosion results: (**a**) erosion rate-time curves, (b) erosion depth after 4 h of testing.

Preprints (www.preprints.org) | NOT PEER-REVIEWED | Posted: 4 November 2020 doi:10.20944/preprints202011.0200.v1

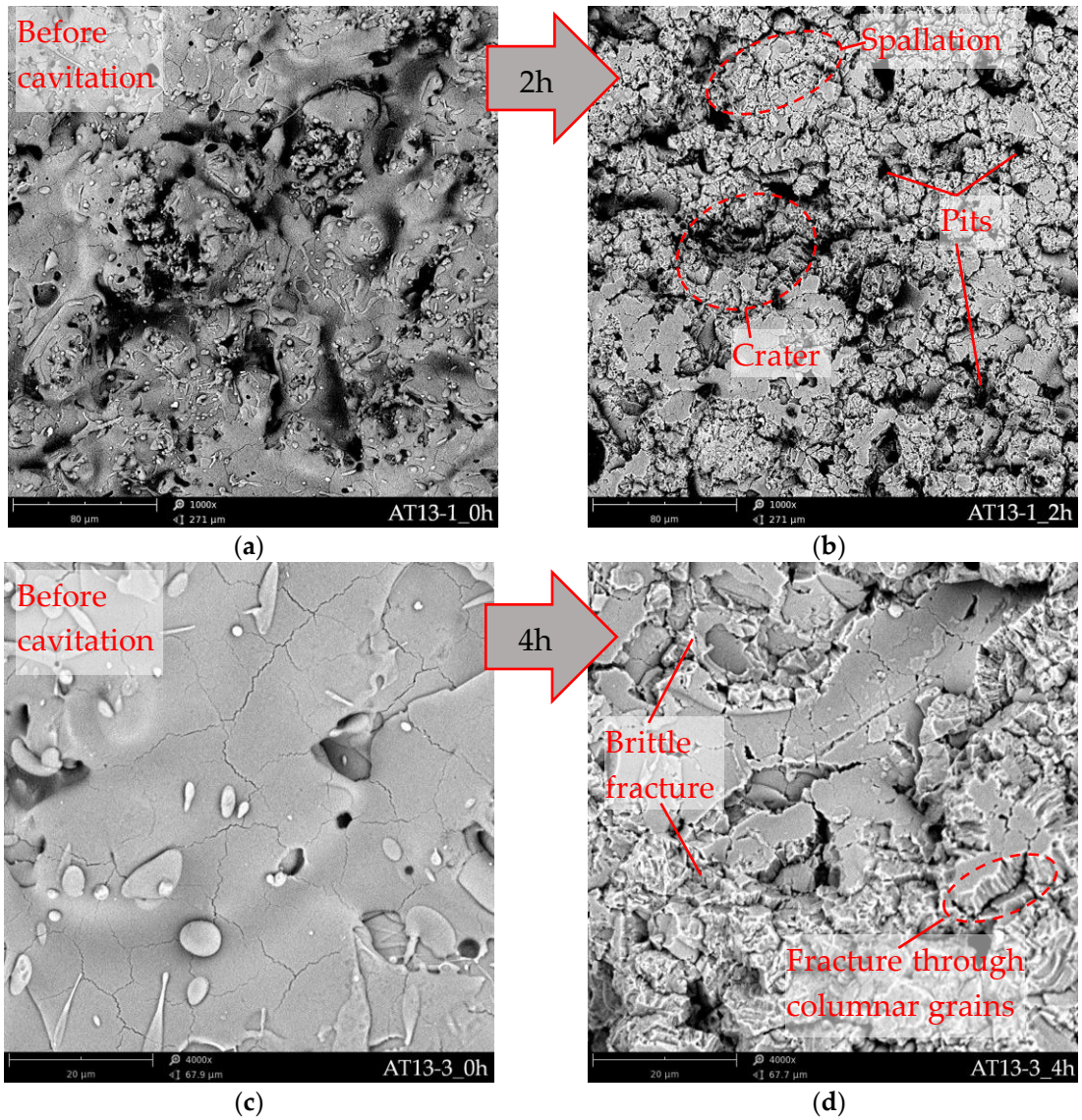

Figure 4. Cavitation damage development observed at different magnifications and exposure times: (**a-b**) progression of erosion in the AT13-1 coating before and after 2 h of cavitation, x1000; (**c-d**) progression of erosion in the AT13-3 coating after 4 h of cavitation testing, x4000, SEM-BSD.

3.1. Model development and process optimization

Figure 5 shows the variations in the fit index depending on the number of neurons in the hidden layer. The fit index was calculated separately for every output network. Considering the learning dataset, it can be seen that the network with 6 or more hidden neurons perfectly matches the measurement data. In the case of the testing dataset, the results are more complicated. On the whole, the network has the best fit to the hardness H and the worst fit to the mean depth of erosion MDE. Taking into account the results for both the learning and testing datasets, we chose the network with the structure 2-6-3, i.e. with 6 neurons in the hidden layer. Figure 3 shows the fit index values for the selected network.

Preprints (www.preprints.org) | NOT PEER-REVIEWED | Posted: 4 November 2020 doi:10.20944/preprints202011.0200.v1

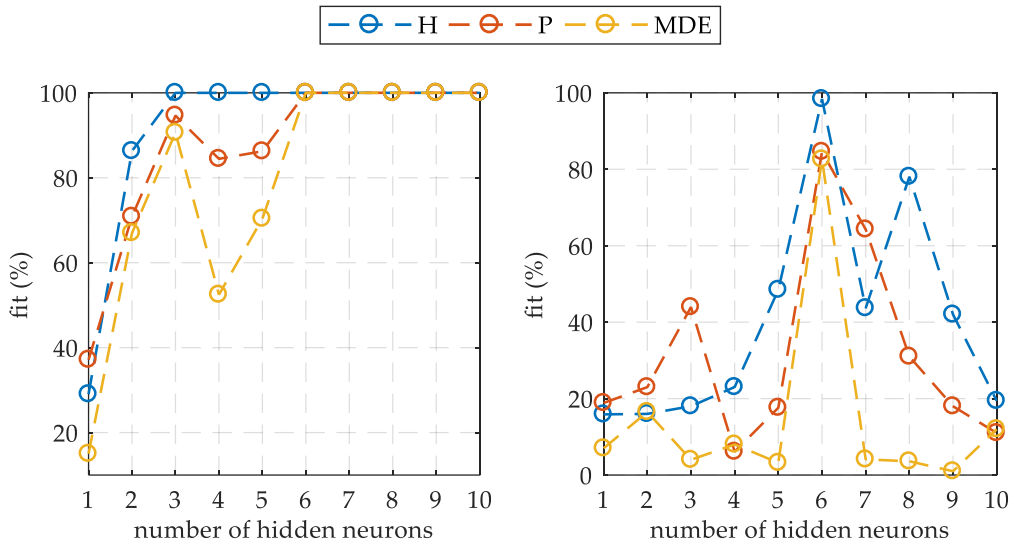

Figure 5. Influence of the number of hidden neurons on the fit index for learning (left) and testing (right) datasets.

Table 3. Fit index for the ANN with a 2-6-3 structure.

Output signal	Fit index (%)	
	Learning dataset	Testing dataset
H	100	98.4
P	100	84.6
MDE	100	82.6

As far as we know, no previous research has investigated the use of ANNs in modelling the hardness, porosity and cavitation wear of APS thermally sprayed coatings. It is, therefore, difficult to provide a basis for comparison with our modelling results. Under the adopted modelling procedure, obtained results indicate that the model yields acceptable accuracy [47].

Based on the ANN, we performed a series of APS thermal spray process simulations using different parameters. The stand-off distance h was changed in the range of 80-100 mm with a step of 1 mm, while the velocity torch ranged from 300 to 500 mm·s^{-1} and was changed with a step of 10 mm·s^{-1}. Figures 6-8 show simulation results.

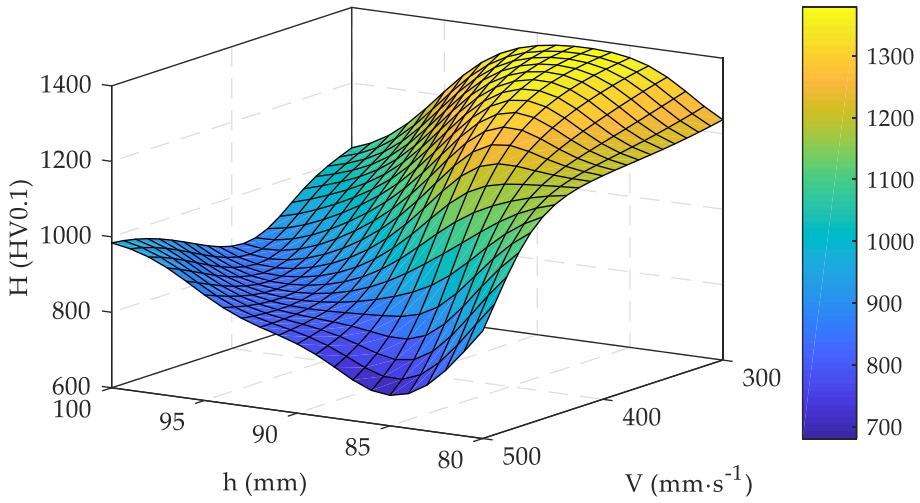

Figure 6. Surface plot of the function H(h, V).

Preprints (www.preprints.org) | NOT PEER-REVIEWED | Posted: 4 November 2020 doi:10.20944/preprints202011.0200.v1

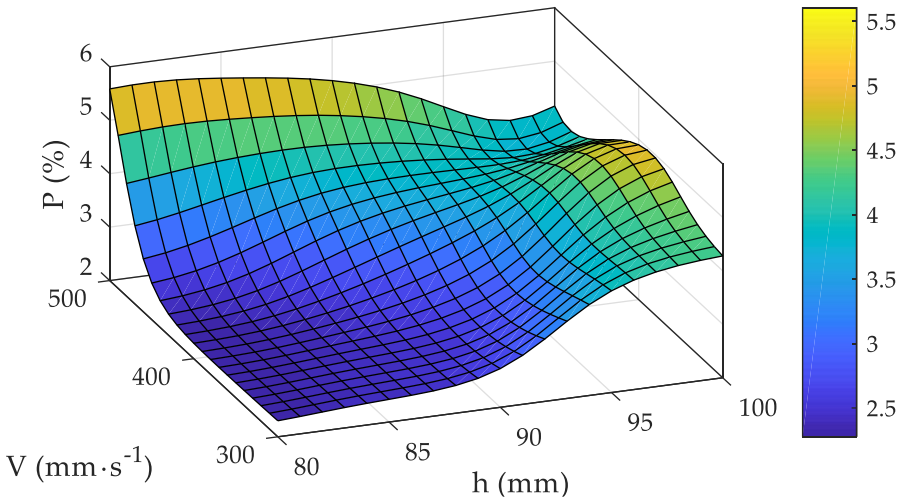

Figure 7. Surface plot of the function P(h, V).

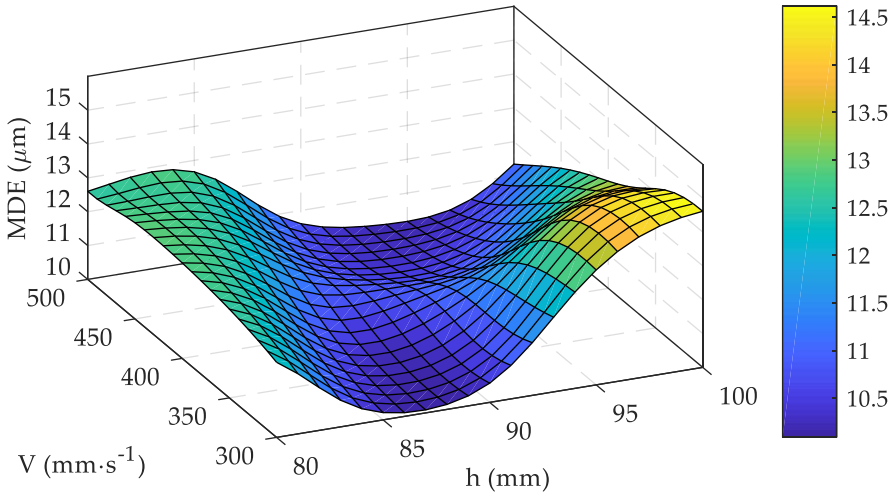

Figure 8. Surface plot of the function MDE(h, V).

An analysis of the data in Figures 6-8 demonstrates it is difficult to determine manually the values of the stand-off distance h and torch velocity V that will yield the optimal value of the objective function J (5). Using MOGA, we have found a set of h and V that forms a Pareto front (Figure 9). The Pareto front is a popular tool for solving various multi-objective optimization problems; it is also successfully used for optimizing coating structure [53, 54]. For clarity, the optimal solutions are shown as contour plots (Figures 10, 11, 12) and are listed in Table 4. Out of all Pareto optimal solutions, the highest hardness and, at the same time, the lowest mean depth of erosion (i.e. 1377 HV0.1 and 10.1 μm, respectively) are obtained with h=86.9 mm, V=304 mm·s^{-1} and h=87.3 mm, V=304 mm·s^{-1}; while the lowest porosity of 2.28% can be observed with h=80 mm, V=371 mm·s^{-1} and h=80.4 mm, V=357 mm·s^{-1}. Summing up, the proposed procedure is essential for future selection of thermal spray process parameters, especially for the design of ceramic coatings with specified functional properties.

Preprints (www.preprints.org) | NOT PEER-REVIEWED | Posted: 4 November 2020 doi:10.20944/preprints202011.0200.v1

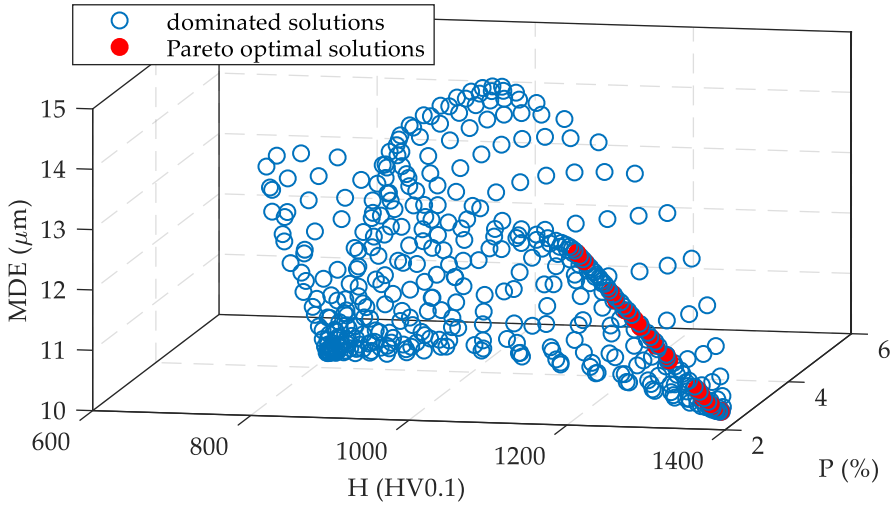

Figure 9. Pareto front in objective space.

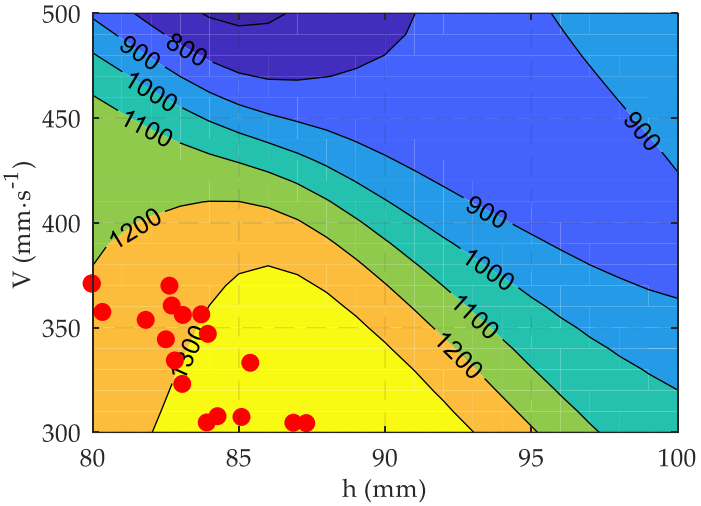

Figure 10. Contour plot of the function H(h, V) with optimal solutions (red dots).

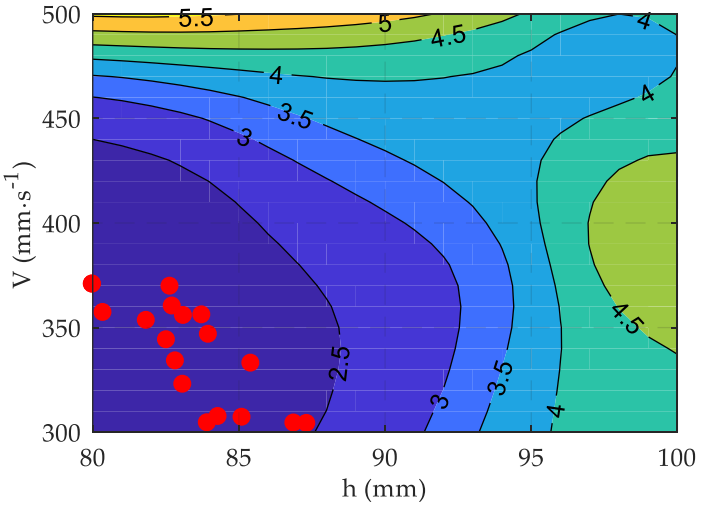

Figure 11. Contour plot of the function P(h, V) with optimal solutions (red dots).

Preprints (www.preprints.org) | NOT PEER-REVIEWED | Posted: 4 November 2020 doi:10.20944/preprints202011.0200.v1

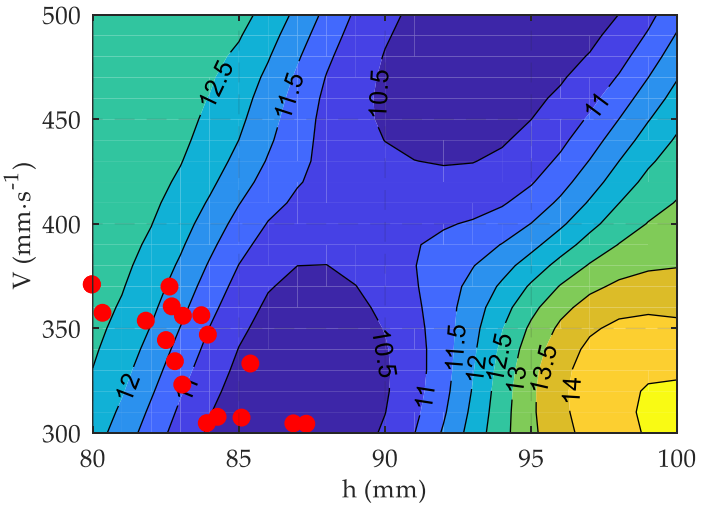

Figure 12. Contour plot of the function MDE(h, V) with optimal solutions (red dots).

Table 4. Set of Pareto-optimal solutions.

Solution number	Decision variables x*		Objective function J		
	h (mm)	V (mm·s^{-1})	H (HV0.1)	P (%)	MDE (μm)
1	80.0	371	1203	2.28	12.7
2	84.0	347	1316	2.38	11.0
3	86.9	304	1377	2.46	10.1
4	82.7	370	1250	2.32	11.9
5	83.7	356	1299	2.36	11.2
6	82.7	360	1263	2.33	11.8
7	80.4	357	1212	2.28	12.6
8	81.8	353	1244	2.31	12.1
9	82.8	334	1294	2.35	11.3
10	85.1	307	1366	2.42	10.2
11	82.5	344	1274	2.33	11.6
12	85.4	333	1356	2.42	10.3
13	83.1	323	1313	2.37	11.0
14	83.9	304	1349	2.40	10.5
15	84.3	307	1354	2.41	10.4
16	83.1	356	1280	2.34	11.5
17	87.3	304	1377	2.48	10.1

4. Conclusions

This study proposed the original neural model and algorithm for optimising atmospheric plasma spray (APS) process parameters to obtain Al_2O_3-13%TiO_2 ceramic coatings with the required porosity and hardness, and thus with the highest cavitation erosion resistance (CER). The results of the study lead to the following conclusions:

1. The APS ceramic coatings exhibit a relatively dense lamellar microstructure with initial cracking of the lamellas, they also contain unmelted feedstock powder and splats built up from columnar grains. The hardness of the coatings ranges from 885 HV0.1 to 1235 HV0.1 and their porosity ranges from 5.59% to 2.30%. The hardness and porosity of the coatings depend on the ASP process parameters.

2. The AT13-3 specimen deposited with h = 90 mm and V = 400 m/s exhibits the highest CER resistance. The cavitation erosion mechanism identified for the coatings relies on brittle fracture propagating through the columnar grains; also, it is accelerated by the presence of coating non-uniformities such as pores, cracks and particles of unmelted material.
3. The selection of APS process parameters to obtain coatings with the required properties is a multicriteria decision problem. The fusion of artificial neural network and genetic algorithm is a novel approach. This promising method can be employed for solving complex problem such as the selection of spray parameters in the design of ceramic coatings with specified hardness, porosity and superior cavitation erosion resistance.
4. By applying the multi-objectives optimization, we found a set of Pareto-optimal solutions. Summing up the optimisation results, the highest hardness and, at the same time, the lowest mean depth of erosion, i.e. 1377 HV0.1 and 10.1 μm, respectively, were obtained with h=86.9 mm, V=304 mm·s^{-1} and h=87.3 mm, V=304 mm·s^{-1}; while the lowest porosity of 2.28% was obtained with h=80 mm, V=371 mm·s^{-1} and h=80.4 mm, V=357 mm·s^{-1}. These parameters are optimal for APS Al_2O_3-13%TiO_2 ceramic coatings.

Author Contributions: Conceptualization, M.S, M.A. and L.Ł.; methodology, M.S, M.A. and L.Ł.; software, M.A.; validation, M.S, M.A. and L.Ł.; formal analysis, M.S, M.A., L.Ł., M.W. and M.M.; investigation, M.S, M.A. and L.Ł.; resources, M.S, M.A., L.Ł., M.W. and M.M.; data curation, M.A.; writing—original draft preparation, M.S, M.A. and L.Ł.; writing—review and editing, M.S, M.A. and L.Ł.; visualization, M.S, M.A. and L.Ł.; supervision, M.S, M.A. and L.Ł.; project administration, M.S.; funding acquisition, M.S, M.A. and L.Ł. All authors have read and agreed to the published version of the manuscript.

Funding: The research was financed in the framework of the project Lublin University of Technology—Regional Excellence Initiative, funded by the Polish Ministry of Science and Higher Education (contract No. 030/RID/2018/19).

Acknowledgments: In this section you can acknowledge any support given which is not covered by the author contribution or funding sections. This may include administrative and technical support, or donations in kind (e.g., materials used for experiments).

Conflicts of Interest: The authors declare no conflict of interest.

References

1. Pawlowski, L. *The Science and Engineering of Thermal Spray Coatings*; 2nd Edition.; Wiley: Chichester, England ; Hoboken, NJ, 2008; ISBN 978-0-471-49049-4.
2. Principles of Thermal Spraying - Plasma-Spray Coating - Wiley Online Library Available online: https://onlinelibrary.wiley.com/doi/10.1002/9783527614851.ch02 (accessed on Sep 17, 2020).
3. *Handbook of Thermal Plasmas - Maher I. Boulos, Pierre L. Fauchais, Emil Pfender - Google Książki*;
4. Lugscheider, E.; Barimani, C.; Eckert, P.; Eritt, U. Modeling of the APS plasma spray process. *Computational Materials Science* **1996**, *7*, 109–114, doi:10.1016/S0927-0256(96)00068-7.
5. Guessasma, S.; Montavon, G.; Coddet, C. Modeling of the APS plasma spray process using artificial neural networks: basis, requirements and an example. *Computational Materials Science* **2004**, *29*, 315–333, doi:10.1016/j.commatsci.2003.10.007.
6. Sahab, A.R.M.; Saad, N.H.; Kasolang, S.; Saedon, J. Impact of Plasma Spray Variables Parameters on Mechanical and Wear Behaviour of Plasma Sprayed Al2O3 3%wt TiO2 Coating in Abrasion and Erosion Application. *Procedia Engineering* **2012**, *41*, 1689–1695, doi:10.1016/j.proeng.2012.07.369.

7. Aruna, S.T.; Balaji, N.; Shedthi, J.; Grips, V.K.W. Effect of critical plasma spray parameters on the microstructure, microhardness and wear and corrosion resistance of plasma sprayed alumina coatings. *Surface and Coatings Technology* **2012**, *208*, 92–100, doi:10.1016/j.surfcoat.2012.08.016.
8. Yugeswaran, S.; Selvarajan, V.; Vijay, M.; Ananthapadmanabhan, P.V.; Sreekumar, K.P. Influence of critical plasma spraying parameter (CPSP) on plasma sprayed Alumina–Titania composite coatings. *Ceramics International* **2010**, *36*, 141–149, doi:10.1016/j.ceramint.2009.07.012.
9. Michalak, M.; Łatka, L.; Sokołowski, P.; Niemiec, A.; Ambroziak, A. The Microstructure and Selected Mechanical Properties of Al2O3 + 13 wt % TiO2 Plasma Sprayed Coatings. *Coatings* **2020**, *10*, 173, doi:10.3390/coatings10020173.
10. Łatka, L.; Niemiec, A.; Michalak, M.; Sokołowski, P. Tribological Properties of Al2O3 + TiO2 Coatings Manufactured by Plasma Spraying. *BIMONTHLY TRIBOLOGIA* **2019**, *283*, 19–24, doi:10.5604/01.3001.0013.1431.
11. Chochowski, A.; Obstawski, P. The use of thermal-electric analogy in solar collector thermal state analysis. *Renewable and Sustainable Energy Reviews* **2017**, *68*, 397–409, doi:10.1016/j.rser.2016.09.116.
12. Aleksiejuk, J.; Chochowski, A.; Reshetiuk, V. Analog model of dynamics of a flat-plate solar collector. *Solar Energy* **2018**, *160*, 103–116, doi:10.1016/j.solener.2017.11.079.
13. Salat, R.; Awtoniuk, M. Black box modeling of PIDs implemented in PLCs without structural information: a support vector regression approach. *Neural Computing and Applications* **2015**, *26*, 723–734, doi:10.1007/s00521-014-1754-2.
14. Chmiel, J.; Jasionowski, R.; Zasada, D. Cavitation erosion and corrosion of pearlitic gray cast iron in non-standardized cavitation conditions. *Solid State Phenomena* **2015**, *225*, 19–24, doi:10.4028/www.scientific.net/SSP.225.19.
15. Cui, Z.D.; Man, H.C.; Cheng, F.T.; Yue, T.M. Cavitation erosion–corrosion characteristics of laser surface modified NiTi shape memory alloy. *Surface and Coatings Technology* **2003**, *162*, 147–153, doi:10.1016/S0257-8972(02)00399-7.
16. Amarendra, H.J.; Chaudhari, G.P.; Nath, S.K. Synergy of cavitation and slurry erosion in the slurry pot tester. *Wear* **2012**, *290–291*, 25–31, doi:10.1016/j.wear.2012.05.025.
17. Wang, Y.; Wu, J.; Ma, F. Cavitation–silt erosion in sand suspensions. *J Mech Sci Technol* **2018**, *32*, 5697–5702, doi:10.1007/s12206-018-1116-6.
18. Su, K.; Wu, J.; Xia, D. Classification of regimes determining ultrasonic cavitation erosion in solid particle suspensions. *Ultrasonics Sonochemistry* **2020**, *68*, 105214, doi:10.1016/j.ultsonch.2020.105214.
19. Silva, F.N. da; Oliveira, P.M. de; Araújo, N.M. da F.T. de S.; Carvalho Filho, E.T. de; Cunha, J.D. da; Silva, D.R. da; Medeiros, J.T.N. de Corrosion-cavitation-erosion: surface morphology study of a carbon steel in a multiphasic saline bath. *Matéria (Rio de Janeiro)* **2019**, *24*, doi:10.1590/s1517-707620190001.0639.
20. Liang, L.; Pang, Y.; Tang, Y.; Zhang, H.; Liu, H.; Liu, Y. Combined wear of slurry erosion, cavitation erosion, and corrosion on the simulated ship surface. *Advances in Mechanical Engineering* **2019**, *11*, 1687814019834450, doi:10.1177/1687814019834450.

21. Tocci, M.; Pola, A.; Girelli, L.; Lollio, F.; Montesano, L.; Gelfi, M. Wear and Cavitation Erosion Resistance of an AlMgSc Alloy Produced by DMLS. *Metals* **2019**, *9*, 308, doi:10.3390/met9030308.
22. Hattori, S.; Ishikura, R. Revision of cavitation erosion database and analysis of stainless steel data. *Wear* **2010**, *268*, 109–116, doi:10.1016/j.wear.2009.07.005.
23. Steller, J. International Cavitation Erosion Test and quantitative assessment of material resistance to cavitation. *Wear* **1999**, *233–235*, 51–64, doi:10.1016/S0043-1648(99)00195-7.
24. Szala, M.; Dudek, A.; Maruszczyk, A.; Walczak, M.; Chmiel, J.; Kowal, M. Effect of atmospheric plasma sprayed TiO2-10% NiAl cermet coating thickness on cavitation erosion, sliding and abrasive wear resistance. *Acta Phys. Pol. A* **2019**, *136*, 335–341, doi:10.12693/APhysPolA.136.335.
25. Jasionowski, R.; Przetakiewicz, D.; Przetakiewicz, W. Cavitation Erosion Resistance of Alloys Used in Cathodic Protection of Hulls of Ships. *Archives of Metallurgy and Materials* **2014**, *59*, 241–245, doi:10.2478/amm-2014-0039.
26. Mann, B.S.; Arya, V. An experimental study to corelate water jet impingement erosion resistance and properties of metallic materials and coatings. *Wear* **2002**, *253*, 650–661, doi:10.1016/S0043-1648(02)00118-7.
27. Krella, A.K.; Zakrzewska, D.E. Cavitation Erosion – Phenomenon and Test Rigs. *Advances in Materials Science* **2018**, *18*, 15–26, doi:10.1515/adms-2017-0028.
28. García, G.L.; López-Ríos, V.; Espinosa, A.; Abenojar, J.; Velasco, F.; Toro, A. Cavitation resistance of epoxy-based multilayer coatings: Surface damage and crack growth kinetics during the incubation stage. *Wear* **2014**, *316*, 124–132, doi:10.1016/j.wear.2014.04.007.
29. Dular, M.; Bachert, B.; Stoffel, B.; Sirok, B. Relationship between cavitation structures and cavitation damage. *Wear* **2004**, *257*, 1176–1184.
30. Szala, M. Application of computer image analysis software for determining incubation period of cavitation erosion – preliminary results. *ITM Web Conf.* **2017**, *15*, 06003, doi:10.1051/itmconf/20171506003.
31. Gireń, B.G. *Kawitacyjne niszczenie warstw ukształtowanych wiązką promieniowania laserowego*; Wydawn. IMP PAN: Gdańsk, 2006;
32. Szala, M.; Łatka, L.; Walczak, M.; Winnicki, M. Comparative Study on the Cavitation Erosion and Sliding Wear of Cold-Sprayed Al/Al2O3 and Cu/Al2O3 Coatings, and Stainless Steel, Aluminium Alloy, Copper and Brass. *Metals* **2020**, *10*, 856, doi:10.3390/met10070856.
33. Will, C.R.; Capra, A.R.; Pukasiewicz, A.G.M.; Chandelier, J. da G.; Paredes, R.S.C. Comparative study of three austenitic alloy with cobalt resistant to cavitation deposited by plasma welding. *Welding International* **2012**, *26*, 96–103, doi:10.1080/09507116.2010.527487.
34. Maksimović, V.M.; Devečerski, A.B.; Došen, A.; Bobić, I.; Erić, M.D.; Volkov-Husović, T. Comparative Study on Cavitation Erosion Resistance of A356 Alloy and A356FA5 Composite. *Trans Indian Inst Met* **2017**, *70*, 97–105, doi:10.1007/s12666-016-0864-1.

35. Hattori, S.; Ishikura, R.; Zhang, Q. Construction of database on cavitation erosion and analyses of carbon steel data. *Wear* **2004**, *257*, 1022–1029, doi:10.1016/j.wear.2004.07.002.
36. Tzanakis, I.; Bolzoni, L.; Eskin, D.G.; Hadfield, M. Evaluation of Cavitation Erosion Behavior of Commercial Steel Grades Used in the Design of Fluid Machinery. *Metall Mater Trans A* **2017**, *48*, 2193–2206, doi:10.1007/s11661-017-4004-2.
37. Gao, G.; Zhang, Z.; Cai, C.; Zhang, J.; Nie, B. Cavitation Damage Prediction of Stainless Steels Using an Artificial Neural Network Approach. *Metals* **2019**, *9*, 506, doi:10.3390/met9050506.
38. Szala, M.; Awtoniuk, M. Neural modelling of cavitation erosion process of 34CrNiMo6 steel. *IOP Conference Series: Materials Science and Engineering* **2019**, *710*, 012016, doi:10.1088/1757-899x/710/1/012016.
39. Jafarzadeh, K.; Valefi, Z.; Ghavidel, B. The effect of plasma spray parameters on the cavitation erosion of Al2O3–TiO2 coatings. *Surface and Coatings Technology* **2010**, *205*, 1850–1855, doi:10.1016/j.surfcoat.2010.08.044.
40. Łatka, L.; Szala, M.; Michalak, M.; Pałka, T. Impact of atmospheric plasma spray parameters on cavitation erosion resistance of Al2O3-13%TiO2 coatings. *Acta Phys. Pol. A* **2019**, *136*, 342–347, doi:10.12693/APhysPolA.136.342.
41. Szala, M.; Awtoniuk, M.; Łatka, L.; Macek, W.; Branco, R. Artificial neural network model of hardness, porosity and cavitation erosion wear of APS deposited Al2O3 -13 wt % TiO2 coatings. *Journal of Physics: Conference Series* **2020**, *In print*.
42. Pierlot, C.; Pawlowski, L.; Bigan, M.; Chagnon, P. Design of experiments in thermal spraying: A review. *Surface and Coatings Technology* **2008**, *202*, 4483–4490, doi:10.1016/j.surfcoat.2008.04.031.
43. Szala, M.; Walczak, M.; Łatka, L.; Gancarczyk, K.; Özkan, D. Cavitation Erosion and Sliding Wear of MCrAlY and NiCrMo Coatings Deposited by HVOF Thermal Spraying. *Advances in Materials Science* **2020**, *20*, 26–38, doi:10.2478/adms-2020-0008.
44. Maruszczyk, A.; Dudek, A.; Szala, M. Research into Morphology and Properties of TiO2 – NiAl Atmospheric Plasma Sprayed Coating. *Advances in Science and Technology Research Journal* **2017**, *11*, 204–210, doi:10.12913/22998624/76450.
45. Łatka, L.; Michalak, M.; Jonda, E. Atmospheric Plasma Spraying of Al2O3 + 13% TiO2 Coatings Using External and Internal Injection System. *Advances in Materials Science* **2019**, *19*, 5–17, doi:10.2478/adms-2019-0018.
46. *ASTM G32-10: Standard Test Method for Cavitation Erosion Using Vibratory Apparatus*; ASTM International: West Conshohocken, Philadelphia: PA, USA, 2010;
47. Tangirala, A.K. *Principles of system identification : theory and practice*; CRC Press: Boca Raton, 2015; ISBN 978-1-4398-9599-3.
48. Łatka, L.; Pawłowski, L.; Winnicki, M.; Sokołowski, P.; Małachowska, A.; Kozerski, S. Review of Functionally Graded Thermal Sprayed Coatings. *Applied Sciences* **2020**, *10*, 5153, doi:10.3390/app10155153.
49. Meghwal, A.; Anupam, A.; Murty, B.S.; Berndt, C.C.; Kottada, R.S.; Ang, A.S.M. Thermal Spray High-Entropy Alloy Coatings: A Review. *J Therm Spray Tech* **2020**, *29*, 857–893, doi:10.1007/s11666-020-01047-0.

 doi:10.20944/preprints202011.0200.v1

50. Yılmaz, R.; Kurt, A.O.; Demir, A.; Tatlı, Z. Effects of TiO2 on the mechanical properties of the Al2O3–TiO2 plasma sprayed coating. *Journal of the European Ceramic Society* **2007**, *27*, 1319–1323, doi:10.1016/j.jeurceramsoc.2006.04.099.
51. Matikainen, V.; Niemi, K.; Koivuluoto, H.; Vuoristo, P. Abrasion, Erosion and Cavitation Erosion Wear Properties of Thermally Sprayed Alumina Based Coatings. *Coatings* **2014**, *4*, 18–36, doi:10.3390/coatings4010018.
52. Davis, J.R. *Handbook of Thermal Spray Technology*; ASM International, 2004; ISBN 978-0-87170-795-6.
53. Coello, C.C.; Lamont, G.B.; Veldhuizen, D.A. van *Evolutionary Algorithms for Solving Multi-Objective Problems*; Genetic and Evolutionary Computation; 2nd ed.; Springer US, 2007; ISBN 978-0-387-33254-3.
54. Chen, Q.; Hu, P.; Pu, J.; Wang, J.H. Sensitivity analysis and multi-objective optimization of double-ceramic-layers thermal barrier system. *Ceramics International* **2019**, *45*, 17224–17235, doi:10.1016/j.ceramint.2019.05.278.